Faraday Discussions

Characterization of Pt-doping effects on nanoparticle emission: A theoretical look at Au24Pt(SH)18 and Au24Pt(C3H7)18

Journal:	*Faraday Discussions*
Manuscript ID	FD-ART-05-2022-000110
Article Type:	Paper
Date Submitted by the Author:	18-May-2022
Complete List of Authors:	Havenridge, Shana; Kansas State University, Chemistry Weerawardene, K. L. Dimuthu; Kansas State University, Chemistry Aikens, Christine; Kansas State University, Chemistry

Characterization of Pt-doping effects on nanoparticle emission: A theoretical look at $Au_{24}Pt(SH)_{18}$ and $Au_{24}Pt(C_3H_7)_{18}$

Shana Havenridge, K. L. Dimuthu M. Weerawardene and Christine M. Aikens*

Department of Chemistry, Kansas State University, Manhattan, Kansas 66506, United States

Abstract

Developments in nanotechnology have made the creation of functionalized materials with atomic precision possible. Thiolate-protected gold nanoclusters, in particular, have become the focus of study in literature as they possess high stability and have tunable structure-property relationships. In addition to adjustments in properties due to differences in size and shape, heteroatom doping has become an exciting way to tune the properties of these systems by mixing different atomic d character from transition metal atoms. $Au_{24}Pt(SR)_{18}$ clusters, notably, have shown incredible catalytic properties, but fall short in the field of photochemistry. The influence of the Pt dopant on the photoluminescence mechanism and excited state dynamics has been investigated by a few experimental groups, but the origin of the differences that arise due to doping has not been clarified thoroughly. In this paper, density functional theory methods are used to analyze the geometry, optical and photoluminescent properties of $Au_{24}Pt(SR)_{18}$ in comparison with $[Au_{25}(SR)_{18}]^{1-}$. Further, as these clusters have shown slightly different geometric and optical properties for different ligands, the analysis is completed with both hydrogen and propyl ligands in order to ascertain the role of the passivating ligands.

Introduction

Atomically precise nanoclusters have excited the science community in part because they possess specific geometric,[1-3] optical[4,5] and photoluminescent[6-8] properties that depend sensitively on the various sizes and shapes of the nanoclusters (NCs). The demand for these NCs is increasing, as they can be controlled with atomic precision, and therefore, they provide an alternative to bulk materials or larger nanomaterials because they have precise electronic and geometric structure.[9-12] A well-known example of this is $[Au_{25}(SR)_{18}]^{1-}$, which was structurally determined by the Murray and Jin groups in 2008.[13,14] Since 2008, experimental and theoretical groups have showed that the properties of this cluster can be tuned for different applications such as photodynamic therapy,[15,16] small molecule activation,[17-19] biosensing,[20,21] and more. The immense applicability of $[Au_{25}(SR)_{18}]^{1-}$ has further trigged a variety of theoretical and experimental studies benchmarking the properties of thiolate-protected nanoclusters with different sizes, shapes, ligands, and charge states.[22-26]

In addition to changing the ligand shell or surface structure of the nanocluster, controlled modification of the metal core via doping has become an exciting new progression of this work. $Au_{24}M(SR)_{18}$ clusters (M = dopant) have become star models in understanding the role of the dopant in thiolate-protected clusters,[27] largely because the parent cluster, $[Au_{25}(SR)_{18}]^{1-}$, has been thoroughly studied.[28-32] Out of the immense number of transition metal dopants, $Au_{24}Pt(SR)_{18}$ stands out, as it is an exceptional catalyst[33] as well as a robust oxidizer.[34] Despite initial difficulties to structurally characterize this cluster, which arises in part due to the similarities between Pt and Au,[34,35] the crystal structure was accomplished by Jin and coworkers in 2012.[36] Since that time, several structures of $Au_{24}Pt(SR)_{18}$ have been used to theoretically and experimentally describe the Au-Pt bonding,[37] the cluster stability,[31] the large catalytic activity,[34]

the optical properties, and more. As the electronic structure of a doped cluster is dictated by the type of dopant, the precise dopant location, and synthetically, by the dopant concentration,[38-40] $Au_{24}Pt(SR)_{18}$ is a perfect model to examine how the properties change with a heteroatom dopant.

One of the reasons that thiolate-protected clusters stand out is their high stability, which can be traced back to geometric and electronic effects that can be understood from the superatom model.[41,42] Analogous to atomic theory, superatomic electrons occupy a set of delocalized superatomic orbitals that possess the symmetries of spherical harmonic functions.[43] For instance, similar to an atomic p orbital, there would be a set of three superatomic P molecular orbitals (MOs) that would be energetically degenerate if the nanocluster has perfect spherical symmetry.[44] These molecular orbitals are usually comprised of 6s contributions from the gold atoms in the core of the nanocluster. In the case of $[Au_{25}(SR)_{18}]^{1-}$, there are eight superatomic electrons that create a S^2P^6 configuration.[45] This configuration is equivalent to the atomic configuration of a noble gas, which is one reason why the cluster is so stable. Neutral $Au_{24}Pt(SR)_{18}$, on the other hand, has a S^2P^4 configuration as a result of the six superatomic electrons present in this system, which results in one empty superatomic P orbital.[19,46] Because that first unoccupied orbital is empty, the first two excited state transitions (P→P) are dipole-forbidden, and hence, $Au_{24}Pt(SR)_{18}$ clusters have shown to have similar absorption trends to $[Au_{25}(SR)_{18}]^{1+}$, as well as similar electron dynamics to the open shell neutral $Au_{25}(SR)_{18}$ cluster.[47] The Pt dopant is thought to accelerate the core-shell coupling, which results in a faster relaxation to the ground state as compared to $[Au_{25}(SR)_{18}]^{1-}$.[48,49]

While there is some literature on how the Pt dopant changes the electron dynamics mechanisms compared to the parent cluster based on 2DES and TA measurements, no experimental photoluminescence (PL) emission peak is present in the range of 600-1600 nm.[50] The reason for the missing emission in Pt-doped clusters is unclear, perpetuating the need for theoretical studies. Further, among the $Au_{24}Pt(SR)_{18}$ literature, several different ligands have been used. Negishi and coworkers showed in 2019 that there is a large difference in geometry as well as optical absorption spectra when R=PET (PET = 2-phenylethanethiolate) and R=TBBT (TBBT = 4-tert-butylbenzenethiolate) in $Au_{24}Pt(SR)_{18}$.[35] While some gold nanoclusters with the same core size have shown similar optical properties between ligands,[51] small nanoclusters such as $Au_{24}Pt(SR)_{18}$ experience a larger influence from the bulkiness of the ligand shell.[40] This paper will therefore provide a theoretical look into the electronic structure, optical, and photoluminescent properties of $Au_{24}Pt(SH)_{18}$ and $Au_{24}Pt(C_3H_7)_{18}$ and examine how the dopant changes the properties compared to $[Au_{25}(SR)_{18}]^{1-}$.

Computational Details

All calculations with $Au_{24}Pt(SH)_{18}$ were performed using the Amsterdam Density Functional (ADF) 2016.101 package, and all calculations of $Au_{24}Pt(C_3H_7)_{18}$ and $[Au_{25}(SC_3H_7)_{18}]^{1-}$ were completed using the ADF 2018.105 package.[52] Several experimental crystal structures of $[Au_{25}(PET)_{18}]^{1-}$ (Refs.[13,14,29,53,54]) with removed phenyl groups were used as initial input structures for the theoretical calculations of $[Au_{25}(SC_3H_7)_{18}]^{1-}$. The lowest energy isomer was initially used with single atom Pt replacements as initial input structures to optimize $Au_{24}Pt(C_3H_7)_{18}$. The core structure was later edited with a more flattened-oblate structure to help the calculation converge. For $Au_{24}Pt(SH)_{18}$, the crystal structure of $[Au_{25}(SR)_{18}]^{1-}$ (Refs. 3,13) with single atom Pt replacements was used as an input structure for all calculations. The $Au_{24}Pt(SR)_{18}$ results are obtained with a neutral charge state to match experiment. Scalar relativistic effects were included by utilizing the zeroth-order regular approximation

(ZORA).[55,56] All calculations were completed at the BP86/DZ level of theory. BP86 is a generalized gradient approximation (GGA) exchange-correlation functional,[57,58] and DZ refers to a double-zeta basis set. Additional calculations are performed at the BP86/TZP level of theory for benchmark purposes, where TZP is a triple-zeta polarized basis set. The structure was optimized in the gas phase for all calculations, and the energy and gradient convergence criteria were tightened to $1x10^{-4}$ Hartree and $1x10^{-3}$ Hartree respectively for geometric accuracy. All calculations had a tightened SCF convergence requirement of $1x10^{-8}$. The theoretical absorption spectrum was calculated with linear response time-dependent density-functional theory (TDDFT),[59] where the vertical excitation energies were convolved with a gaussian fit with a full-width half-maximum (FWHM) of 0.15 eV. TDDFT analytical excited state gradients[60] were used to optimize the S_1-S_{21} states for R=H and R=C_3H_7 using the same convergence criteria and level of theory as the ground state. All pictures of the molecular orbitals were created with the ADF graphical user interface (GUI) and presented with a contour value of 0.015.

Results and Discussion

A. Geometric Structure

$Au_{24}Pt(SR)_{18}$ has the same general shape as $[Au_{25}(SR)_{18}]^{1-}$ and is composed of a 13 atom 'icosahedron' core with 6 Au_2S_3 motifs that protect the core by forming rigid V-shaped S-Au-S-Au-S staples that are further protected by organic ligands. It has been shown that the Pt dopant prefers the center position in the core of the nanocluster.[27,35,37,45] This paper additionally supports the conclusion that the Pt dopant prefers the center of the core; energies at the BP86/DZ and BP86/TZP levels of theory are provided in table S1 for various isomers with R=C_3H_7. For simplicity, the term 'icosahedron' refers to the general shape of the core, even though the core of $Au_{24}Pt(SR)_{18}$ is not made up of 20 equivalent equilateral triangles but more of a flattened triangle base, as seen by figure S1. This breaking of spherical symmetry creates a distorted oblate ellipsoid[61] and is a direct result of the Jahn-Teller effect, which occurs because the P orbitals are not completely filled.[62] The core distortion from the dopant is more prominent with the larger ligand, and in fact, this geometric change between ligands can be qualitatively observed in pictures (figure 1). The optimized ground state (S_0) structures in both clusters experience an elongation of two specific Au core – Pt center bonds that have an average distance of 2.850 Å in $Au_{24}Pt(SH)_{18}$ and 2.940 Å in $Au_{24}Pt(C_3H_7)_{18}$. With the larger C_3H_7 ligand these two bonds are ~0.11 Å larger than the rest of the Au core – Pt center bonds, whereas in $Au_{24}Pt(SH)_{18}$, the elongated bonds are only 0.03 Å larger than the rest of the Au center – Pt bonds.

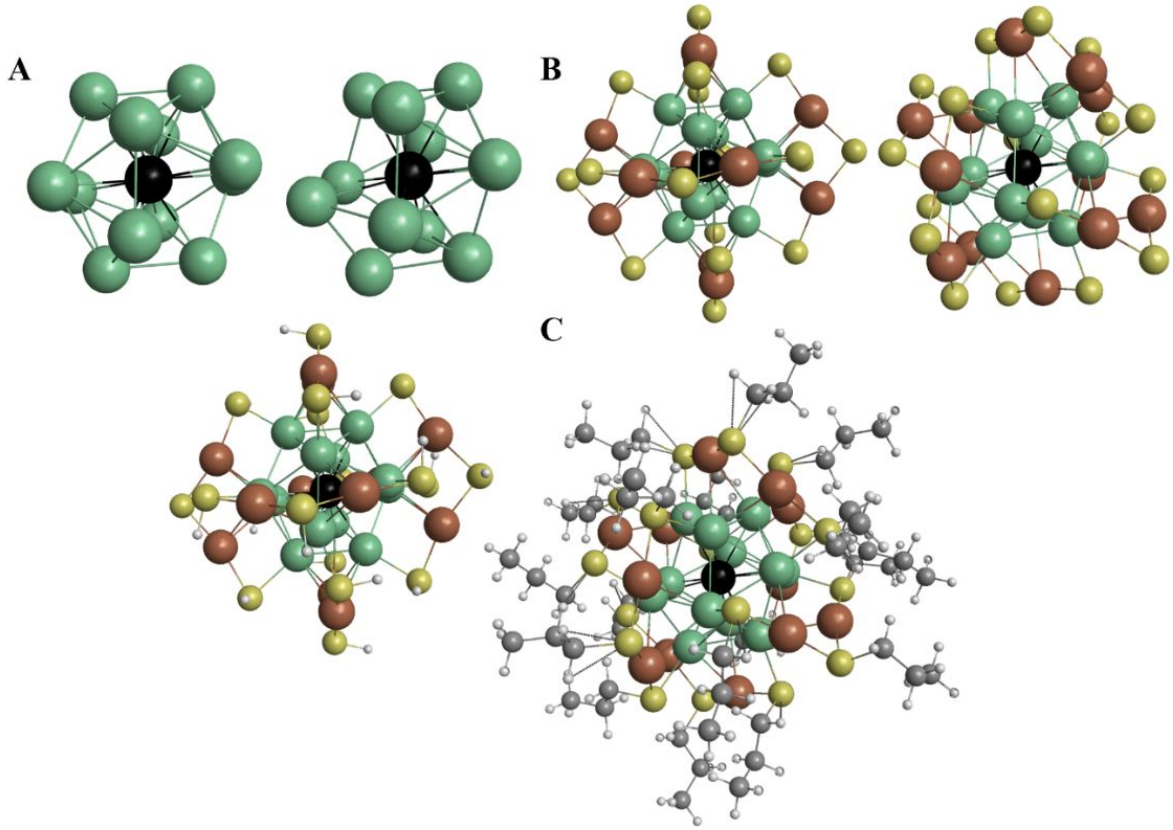

Figure 1. Optimized ground state geometry of $Au_{24}Pt(SR)_{18}$ with R = H (left) and R = C_3H_7 (right). Color scheme: black = Pt, green = Au core atoms, brown = Au shell atoms, yellow = S, grey = C, and white = H. (A) Distorted 'icosahedron' $Au_{12}Pt$ core. (B) $Au_{12}Pt$ core protected by six Au_2S_3 staples. (C) Full $Au_{24}Pt(SR)_{18}$ cluster with the different ligands.

Despite the almost identical average Au-S-C angle of 103.7° for $[Au_{25}(SC_3H_7)_{18}]^{1-}$ and $Au_{24}Pt(SC_3H_7)_{18}$ at the BP86/DZ level of theory, the orientation of the propyl groups changes in one S-Au-S staple. To be more specific, in the lowest energy isomer of $[Au_{25}(SC_3H_7)_{18}]^{1-}$, the propyl groups attach to the Au_2S_3 staples in alternating cis/trans configurations, exhibited in figure S2.[63] In $Au_{24}Pt(SC_3H_7)_{18}$, one of the Au_2S_6 staples has a trans/trans orientation rather than a cis/trans orientation. As a consequence of this change, the propyl groups attached to two nearby staples create gauche/gauche/anti and gauche/anti/anti configurations, which is quite different from the all-anti configuration that is present in the propyl groups of the $[Au_{25}(SC_3H_7)_{18}]^{1-}$ cluster. This shows that not only does the Pt atom distort the core, but also the shell of the nanocluster, the attachment of the propyl groups to the shell, and the configurations of the propyl groups themselves. In 2019, it was found that the interaction between phenyl groups in the TBBT ligand leads to a higher symmetry as compared to the PET ligand.[35] The work demonstrated that with that higher symmetry ligand (TBBT), the metal core shrinks. This same relationship is seen between hydrogen and propyl groups as the Pt center-Au core and Au core-Au core bonds both shrink ~0.03 Å with the more symmetric ligand (R=H). Despite the difference in electronic structure, the average bond distances in $Au_{24}Pt(SH)_{18}$ and $[Au_{25}(SR)_{18}]^{1-}$ are very similar, differing less than 0.006 Å in the core/shell as seen in table 1. $Au_{24}Pt(SC_3H_7)_{18}$, on the other hand, differs quite a bit more compared to $[Au_{25}(SR)_{18}]^{1-}$: ~0.03 Å in the core and

~0.02 Å in the Au-S and S-S bonds. While the Jahn-Teller effects are still present in $Au_{24}Pt(SH)_{18}$, the symmetry distortion is more exaggerated with the larger ligand.

Table 1. Average bond distances (Å) and standard deviation (Å) of the core and shell atoms at the BP86/DZ ground state geometry. The atom labels are given in figure S3.

(Å)	Au/Pt Center-Au Core	Au Core-Au Core	Au Core-Au Shell	Au Core-S Terminal	Au Shell-S Staple	S-S Distance
$[Au_{25}(SC_3H_7)_{18}]^{1-}$	2.830	2.973	3.121	2.539	2.430	4.821
	0.014	0.100	0.130	0.005	0.009	0.008
$Au_{24}Pt(SH)_{18}$	2.827	2.974	3.115	2.516	2.422	4.809
	0.016	0.189	0.119	0.023	0.005	0.006
$Au_{24}Pt(C_3H_7)_{18}$	2.853	3.003	3.133	2.523	2.424	4.817
	0.054	0.256	0.157	0.030	0.008	0.009

B. Electronic Structure

These large geometric changes between the parent and the doped cluster originate from the breaking of spherical symmetry of the superatomic orbitals. As illustrated through the molecular orbital (MO) diagram in figure S4, the HOMO and HOMO-1 MOs are essentially degenerate in $Au_{24}Pt(SH)_{18}$, only differing by 0.03 eV. The larger symmetry distortion in $Au_{24}Pt(SC_3H_7)_{18}$ results in a larger splitting of the HOMO and HOMO-1 MOs, which have a difference in energy of 0.11 eV. The empty superatomic P MO differs significantly in energy from the two other P MOs that are occupied. $Au_{24}Pt(SR)_{18}$ clusters have a completely different electronic structure than $[Au_{25}(SR)_{18}]^{1-}$ because of this difference in P superatomic MO occupation. This results in much smaller HOMO (H) – LUMO (L) gaps of 0.37 eV and 0.42 eV for $Au_{24}Pt(SR)_{18}$ with R=H and R=C_3H_7, respectively, compared to a H-L gap of 1.11 eV in $[Au_{25}(SC_3H_7)_{18}]^{1-}$. Images of the first six frontier MOs for the Pt-doped systems (H-2 through L+2) can be seen in figure S5.

C. Optical Absorption Spectra

In the literature, the energy of the main peak for $Au_{24}Pt(SR)_{18}$ clusters has ranged from 2.07 – 2.12 eV,[33-35,64] with two other optical features of note: one broad band in the IR range, and one high energy shoulder on the edge of the UV spectrum. These three spectral features are similar to those seen in $[Au_{25}(SR)_{18}]^q$ clusters (q = -1,0,+1), where the anionic cluster has a high energy shoulder around 403 nm (3.08 eV), a peak at 450 nm (2.76 eV) and a broad peak around 680 nm (1.81 eV).[62] When the cluster starts to lose electrons, i.e. goes from the anionic to cationic cluster, and hence goes from a fully filled P shell to an empty P shell, the shoulder has slightly higher energy at 3.15 eV, the main peak redshifts to about 2.58 eV, and the broad band blue-shifts to ~1.88 eV.[29] Similar optical shifts are also seen with the Pt atom as $Au_{24}Pt(SR)_{18}$ clusters have an experimental high energy shoulder at 400 nm (3.10 eV) that slightly blueshifts compared to $[Au_{25}(SR)_{18}]^{1-}$, and the main peak is redshifted to 2.10 eV.[36,61] At the BP86/DZ level of theory, the spectral shape between the experimental absorption spectrum and theory matches almost identically as seen in figure S6. Depending on the ligand, the high energy shoulder is around 420 or 450 nm (2.76 or 2.95 eV), the main peak is around 550-590 nm (2.1-2.25 eV) and the broad peak at the lower energy park of the spectrum is in the 700-900 nm range (1.37-1.77 eV).

The low energy peak attributed to the band from 770-870 nm is a combination of two dominant excitations for each nanocluster. The two strongest transitions in this energy range lie at 1.62 eV and 1.66 eV for R=H (table 2), which are S_{20} and S_{21} for this system (table S2). The two strongest transitions for R=C_3H_7, are a little more split, with excitation energies of 1.43 and 1.54 eV (table 2), which are S_{14} and S_{17} for this system. For both ligands, the lower energy peak arises as a result of an excitation between an occupied superatomic P MO (H or H-1) to one of the two lowest energy superatomic D virtual MOs (L+1 or L+2). In the propyl ligand, an additional transition from a MO with large d-atomic orbital contributions from the gold atoms (H-13) transitions into the empty P LUMO which starts to mix with the P→D transition. This mixing is only present with the larger ligand. In general, the propyl system exhibits more mixing and splitting, which is likely due to its greater geometrical distortion from an idealized icosahedral core.

The dominant peak observed in the spectrum, corresponding to the ~600 nm experimental peak, is very different between the two ligands (figure 2). For the propyl ligand, there is one dominant excitation at 2.17 eV that makes up the peak with mixed P→D and d→P character, whereas for hydrogen, there are several excitations around 2.20 eV that make up the peak. The excitation with the largest oscillator strength lies at 2.30 eV and is made up of a dominant P→D transition. To observe the differences from the Pt dopant, the absorption energies for S_1-S_{21} were calculated at the BP86/DZ level of theory, along with the type of transitions responsible for each excitation (table S2). Only the first 21 states were analyzed in detail; however, the first 1500 excitations were calculated to create the full theoretical spectrum (figure S6). It is worth noting that the first two excitations, S_1 and S_2, for $Au_{24}Pt(SR)_{18}$ originate from dipole-forbidden transitions (P→P). These transitions are present in the theoretical spectrum at 0.42 eV and 0.45 eV or 0.47 eV and 0.59 eV for the hydrogen and propyl groups, respectively. In comparison, $[Au_{25}(SC_3H_7)_{18}]^{1-}$ has three vertical excitations that make up the first peak, and all of these excitations arise from P→D transitions. The excitation with the largest oscillator strength is at 1.36 eV, which is a slightly lower absorption energy than the first peak with the Pt dopant. Other density functional theory (DFT) studies resulted in an absorption energy of 1.32 eV for $[Au_{25}(SC_3H_7)_{18}]^{1-}$ at the same level of theory, which matches well with our work.[63]

Table 2. Absorption details of the vertical excitation energies that make up the dominant peaks in the absorption spectrum (figure 2) at the BP86/DZ level of theory in $Au_{24}Pt(SR)_{18}$ for R = H and R = C_3H_7.

Peak	Peak Energy (eV)	Oscillator Strength (a.u.)	Major Transitions	Transition Type
R = Hydrogen (a)	1.62	2.19 x 10^{-2}	H→L+2 H-1→L+1	P→D P→D
R = Hydrogen (b)	1.66	2.20 x 10^{-2}	H-1→L+2	P→D
R = Hydrogen (c)	2.30	1.22 x 10^{-2}	H-1→L+4	P →D
R = Propyl (a)	1.43	2.31 x 10^{-2}	H-1→L+1 H→L+2	P→D P→D
R = Propyl (b)	1.54	2.12 x 10^{-2}	H-1→L+2 H-13→L	P→D d→P
R = Propyl (c)	2.17	2.89 x 10^{-2}	H-1→L+4 H-30→ L	P→D d→P

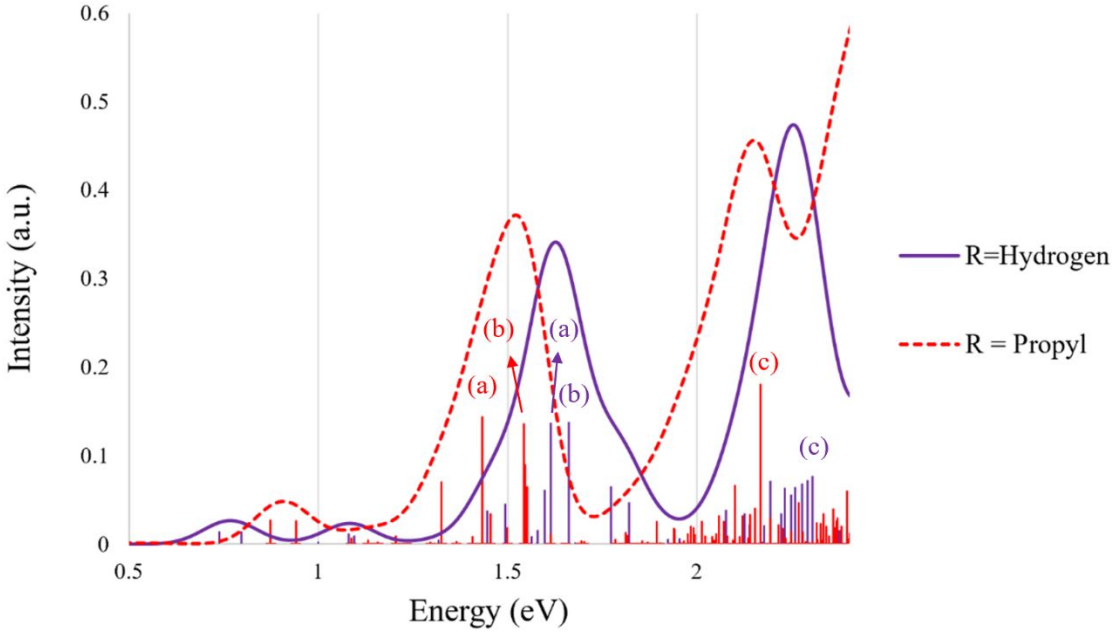

Figure 2. TDDFT absorption spectrum at the BP86/DZ level of theory for $Au_{24}Pt(SR)_{18}$ with R = H (solid purple) and R = C_3H_7 (dotted red).

D. Emission

In 2016, the S_1 state of $[Au_{25}(SR)_{18}]^{1-}$ was reported to be the emissive state originating from a superatomic P→D transition in the core of the nanocluster.[63] Because the S_1 state arises from P→P transitions in $Au_{24}Pt(SR)_{18}$ clusters, these clusters will undergo a very different PL mechanism from the $[Au_{25}(SR)_{18}]^{1-}$ cluster. Excited state optimization calculations on the S_1 and S_2 excited states of the $Au_{24}Pt(SR)_{18}$ clusters failed due to near-degeneracies with the ground state, which indicate that a conical intersection is nearby. Nonradiative relaxation occurs quickly near conical intersections, so these findings indicate that the S_1 and S_2 states are unlikely to yield emission with an appreciable quantum yield. This conical intersection likely occurs because the P orbitals that provided the HOMO and LUMO in the ground state can become degenerate once the nanocluster has appropriately distorted during the excited state relaxation process. To examine the PL mechanism further, higher excited state geometry optimizations were completed. Two states (S_3, S_{19}) in $Au_{24}Pt(SC_3H_7)_{18}$ and three states (S_{15}, S_{18}, S_{21}) out of the first 21 in $Au_{24}Pt(SH)_{18}$ converged geometrically to our chosen criteria, rather than failing due to quasidegeneracies with the next lower energy excited state. Out of the five minima found for the two clusters, three of the excited states originate from d→P transitions (S_3, S_{15}, S_{18}, S_{19}). Some of these excited states have optimized HOMO-LUMO gaps that are less than 0.10 eV (table 3). Of note, the S_{15}, S_{18} and S_{19} states have very small energy gaps between the optimized excited state geometries and the state below (denoted as *n*-1, where *n* is the optimized excited state). A smaller energetic gap between orbitals leads to more efficient coupling of the excited state with the ground state, promoting a nonradiative transition over the emission of a photon.[48] Thus, the system is unlikely to remain in these geometries for any significant amount of time. The $S_n - S_{n-1}$ gap is a little larger for the S_3 state, at 0.28 eV. Even though we were unable to fully converge the S_3 geometry when R=H, we observe a similar energy gap between S_3 and S_2. The separation between the S_3 and the S_2 state could potentially be large enough to observe emission; however, this emission is predicted to be very low in energy (< 0.51 eV) and may be outside of typical experimental windows.

The S_{21} state is unique, originating from a dipole allowed P→D transition with a predicted emission energy of 1.52 eV. At the optimized S_{21} geometry, the nanocluster has a relatively large HOMO-LUMO gap of 0.23 eV. This value is not as large as the optimized H-L gap in the S_1 state of $[Au_{25}(SR)_{18}]^{1-}$ (0.83 eV);[63] however, the energy gap could be large enough to potentially emit a photon. At the optimized S_{21} state, however, the S_{20} energy only differs by 0.002 eV from the S_{21} energy. As the energy difference is negligible between the two states, it is likely that a system in the S_{21} state would quickly cross to the S_{20} state. While likely not an emissive minimum, the S_{21} state does have a more unique electronic structure than the other excited state minima. The purely radiative lifetime of the S_{21} state is predicted to be 0.42 μs, which is ~45x faster than the radiative lifetime value of 19.36 μs from the S_1 state in $[Au_{25}(SR)_{18}]^{1-}$, predicted by the Fermi-Golden rule. Geometrically, the there is no notable difference between the S_0 and S_{21} states, as each type of bond changes less than 0.005 Å (table S3).

Overall, this work shows that all the minima found from the first 21 excited singlet states would likely exhibit nonradiative relaxation rather than the emission of a photon, and therefore, these findings indicate that there is not an emissive state for the $Au_{24}Pt(SR)_{18}$ cluster in the 600-1600 nm energy range. Transient absorption and other pump/probe experiments have been used to try and gain insights into the excited state relaxation mechanism by exciting higher energy states. These studies have concluded that excited state deactivation includes ultrafast (~0.6 ps)

relaxation within the core states, several picoseconds of core relaxation to surface states, followed by slow relaxation (>1 ns) back to the ground state.[47] Further, it was shown that the core states should not contribute to the TA signal after 30 ps.[49] The present theoretical work indicates that there are no charge transfer surface or 'trap' states between the superatomic core states, but there are no likely candidates for singlet states that would undergo radiative relaxation. The full picture of electronic relaxation in the $Au_{24}Pt(SR)_{18}$ nanocluster is not complete without a nonradiative analysis, which would require nonadiabatic calculations that are outside the scope of this work.

Table 3. Emission information for $Au_{24}Pt(SR)_{18}$ with R = H and R = C_3H_7 from converged minima on different excited state potential energy surfaces as calculated by TDDFT at the BP86/DZ level of theory. $S_n - S_{n-1}$ gap refers to the difference in emission energy of the state with the state below it at the optimized geometry in the table. The calculated Stokes shift is reported with respect to the vertical excitation energy of the main peak (i.e., 2.30 eV and 2.17 eV for R = H and R = C_3H_7, respectively) for consistency.

S_n	S_3	S_{15}	S_{18}	S_{19}	S_{21}
Ligand	R=Propyl	R=H	R=H	R = Propyl	R=H
Emission energy (eV)	0.51	1.25	1.34	1.41	1.52
Stokes shift (eV)	1.66	1.05	0.96	0.76	0.78
Lifetime (μs)	51.4	1.46	45.5	0.38	0.42
$S_n - S_{n-1}$ Gaps (eV)	0.278	0.030	0.025	0.000	0.002
H-L Gap (eV)	0.08	0.04	0.02	0.28	0.23
Transition Origin	d→P	d→P	d→P	d→P	P→D

Conclusion

Heteroatom dopants have provided a new way to tune the geometric, optical and photoluminescent properties of atomically precise thiolate protected gold nanoclusters for several different applications. Known for their large catalytic ability, $Au_{24}Pt(SR)_{18}$ clusters provide a good example of how the distortion from a different superatomic electron count directly changes the properties of $[Au_{25}(SR)_{18}]^{1-}$. (TD)DFT calculations were performed to investigate these changes in the gas phase. Geometrically, the dopant distorts the parent cluster from an icosahedron to an ellipsoid, redshifts the absorption energy of the main peak and quenches the photoluminescence. Replacing the small hydrogen groups with a bulkier ligand, such as propyl, creates more distortion in the core/shell structure both geometrically and electronically, and redshifts the absorption energy. Higher excited state calculations suggest that there is not an emissive electronic state due to the small energy gaps between orbitals, but instead, nonradiative relaxation mechanisms are expected to dominate in the excited state dynamics mechanism. No charge-transfer or surface states are observed in this work, which suggests that the change in the superatomic P electron count in the electronic structure of the core is the primary origin for the change in photoluminescence properties observed between the doped and parent cluster.

Acknowledgment
The authors thank Ken Knappenberger, Chris Ackerson, Flavio Maran and coworkers for conversations that inspired this investigation. S.H., K.L.D.M.W. and C.M.A. were supported by the National Science Foundation (CHE-1905048, CHE-1507909) of the United States. The computing for this work was performed on the Beocat Research Cluster at Kansas State University, which is funded in part by NSF grants CHE-1726332, CNS-1006860, EPS-1006860, and EPS-0919443.

Supplementary Material:
See supporting information for atom definitions, relative energies between dopant positions, molecular orbital diagrams, frontier molecular orbitals, absorption information and optimized coordinates with R=H and R=C_3H_7.

Data Availability Statement:
The data that support the findings of this study are available from the corresponding author upon reasonable request.

Author Information
Corresponding Author
*E-mail: cmaikens@ksu.edu. Phone: 785-532-0954. Fax: 785-532-6666.
Note-- The authors declare no competing financial interest

References
[1] I.L. Garzón, K. Michaelian, M.R. Beltrán, A. Posada-Amarillas, P. Ordejón, E. Artacho, D. Sánchez-Portal, J.M. Soler. Lowest Energy Structures of Gold Nanoclusters. *Physical Review Letters.* 1998, **81,** 1600-1603.
[2] Y.H. Chui, G. Grochola, I.K. Snook, S.P. Russo. Molecular dynamics investigation of the structural and thermodynamic properties of gold nanoclusters of different morphologies. *Physical Review B.* 2007, **75,** 033404.
[3] W. Huang, M. Ji, C.-D. Dong, X. Gu, L.-M. Wang, X.G. Gong, L.-S. Wang. Relativistic Effects and the Unique Low-Symmetry Structures of Gold Nanoclusters. *ACS Nano.* 2008, **2,** 897-904.
[4] M. Zhou, C. Zeng, Q. Li, T. Higaki, R. Jin. Gold Nanoclusters: Bridging Gold Complexes and Plasmonic Nanoparticles in Photophysical Properties. *Nanomaterials.* 2019, **9**.
[5] M. Zhou, R. Jin. Optical Properties and Excited-State Dynamics of Atomically Precise Gold Nanoclusters. *Annual Review of Physical Chemistry.* 2021, **72,** 121-142.
[6] M.Y. Sfeir, H. Qian, K. Nobusada, R. Jin. Ultrafast Relaxation Dynamics of Rod-Shaped 25-Atom Gold Nanoclusters. *The Journal of Physical Chemistry C.* 2011, **115,** 6200-6207.
[7] Q. Li, D. Zhou, J. Chai, W.Y. So, T. Cai, M. Li, L.A. Peteanu, O. Chen, M. Cotlet, X. Wendy Gu, H. Zhu, R. Jin. Structural distortion and electron redistribution in dual-emitting gold nanoclusters. *Nature Communications.* 2020, **11,** 2897.
[8] Q. Li, C.J. Zeman, G.C. Schatz, X.W. Gu. Source of Bright Near-Infrared Luminescence in Gold Nanoclusters. *ACS Nano.* 2021, **15,** 16095-16105.
[9] Z. Hens, J. De Roo. Atomically Precise Nanocrystals. *Journal of the American Chemical Society.* 2020, **142,** 15627-15637.

[10] T. Kawawaki, Y. Negishi. Gold Nanoclusters as Electrocatalysts for Energy Conversion. 2020.
[11] H. Li, C. Zhou, E. Wang, X. Kang, W.W. Xu, M. Zhu. An insight, at the atomic level, into the intramolecular metallophilic interaction in nanoclusters. *Chemical Communications.* 2022, **58,** 5092-5095.
[12] M.F. Matus, H. Häkkinen. Atomically Precise Gold Nanoclusters: Towards an Optimal Biocompatible System from a Theoretical–Experimental Strategy. *Small.* 2021, **17,** 2005499.
[13] M.W. Heaven, A. Dass, P.S. White, K.M. Holt, R.W. Murray. Crystal Structure of the Gold Nanoparticle $[N(C_8H_{17})_4][Au_{25}(SCH_2CH_2Ph)_{18}]$. *Journal of the American Chemical Society.* 2008, **130,** 3754-3755.
[14] M. Zhu, C.M. Aikens, F.J. Hollander, G.C. Schatz, R. Jin. Correlating the Crystal Structure of A Thiol-Protected Au_{25} Cluster and Optical Properties. *Journal of the American Chemical Society.* 2008, **130,** 5883-5885.
[15] H. Kawasaki, S. Kumar, G. Li, C. Zeng, D.R. Kauffman, J. Yoshimoto, Y. Iwasaki, R. Jin. Generation of Singlet Oxygen by Photoexcited $Au_{25}(SR)_{18}$ Clusters. *Chemistry of Materials.* 2014, **26,** 2777-2788.
[16] S. Miyata, H. Miyaji, H. Kawasaki, M. Yamamoto, E. Nishida, H. Takita, T. Akasaka, N. Ushijima, T. Iwanaga, T. Sugaya. Antimicrobial photodynamic activity and cytocompatibility of $Au_{25}(SR)_{18}$ clusters photoexcited by blue LED light irradiation. *Int J Nanomedicine.* 2017, **12,** 2703-2716.
[17] Y. Zhu, R. Jin, Y. Sun. Atomically Monodisperse Gold Nanoclusters Catalysts with Precise Core-Shell Structure. *Catalysts.* 2011, **1**.
[18] D. Yang, Y. Sun, X. Cai, W. Hu, Y. Dai, Y. Zhu, Y. Yang. Catalytic Conversion of C1 Molecules on Atomically Precise Metal Nanoclusters. *CCS Chemistry.* 2022, **4,** 66-94.
[19] G. Hu, Q. Tang, D. Lee, Z. Wu, D.-e. Jiang. Metallic Hydrogen in Atomically Precise Gold Nanoclusters. *Chemistry of Materials.* 2017, **29,** 4840-4847.
[20] P.N. Gunawardene, J.F. Corrigan, M.S. Workentin. Golden Opportunity: A Clickable Azide-Functionalized $[Au_{25}(SR)_{18}]^-$ Nanocluster Platform for Interfacial Surface Modifications. *Journal of the American Chemical Society.* 2019, **141,** 11781-11785.
[21] Y. Xiao, Z. Wu, Q. Yao, J. Xie. Luminescent metal nanoclusters: Biosensing strategies and bioimaging applications. *Aggregate.* 2021, **2,** 114-132.
[22] W. Kurashige, Y. Niihori, S. Sharma, Y. Negishi. Recent Progress in the Functionalization Methods of Thiolate-Protected Gold Clusters. *The Journal of Physical Chemistry Letters.* 2014, **5,** 4134-4142.
[23] R.D. Senanayake, E.B. Guidez, A.J. Neukirch, O.V. Prezhdo, C.M. Aikens. Theoretical Investigation of Relaxation Dynamics in $Au_{38}(SH)_{24}$ Thiolate-Protected Gold Nanoclusters. *The Journal of Physical Chemistry C.* 2018, **122,** 16380-16388.
[24] L. Shaltiel, A. Shemesh, U. Raviv, Y. Barenholz, Y. Levi-Kalisman. Synthesis and Characterization of Thiolate-Protected Gold Nanoparticles of Controlled Diameter. *The Journal of Physical Chemistry C.* 2019, **123,** 28486-28493.
[25] R. Antoine. Supramolecular Gold Chemistry: From Atomically Precise Thiolate-Protected Gold Nanoclusters to Gold-Thiolate Nanostructures. *Nanomaterials.* 2020, **10**.
[26] Z. Meng. Excited-State Dynamics of Large-Sized Thiolate-Protected Au_n (n>100) Nanoclusters. *Progress in Physics.* 2022, **42,** 17-26.

[27] F. Alkan, P. Pandeya, C.M. Aikens. Understanding the Effect of Doping on Energetics and Electronic Structure for Au_{25}, Ag_{25}, and Au_{38} Clusters. *The Journal of Physical Chemistry C.* 2019, **123,** 9516-9527.
[28] H. Qian, C. Liu, R. Jin. Controlled growth of molecularly pure $Au_{25}(SR)_{18}$ and $Au_{38}(SR)_{24}$ nanoclusters from the same polydispersed crude product. *Science China Chemistry.* 2012, **55,** 2359-2365.
[29] M.A. Tofanelli, K. Salorinne, T.W. Ni, S. Malola, B. Newell, B. Phillips, H. Häkkinen, C.J. Ackerson. Jahn-Teller effects in $Au_{25}(SR)_{18}$. *Chem Sci.* 2016, **7,** 1882-1890.
[30] X. Kang, H. Chong, M. Zhu. $Au_{25}(SR)_{18}$: the captain of the great nanocluster ship. *Nanoscale.* 2018, **10,** 10758-10834.
[31] W. Fei, S. Antonello, T. Dainese, A. Dolmella, M. Lahtinen, K. Rissanen, A. Venzo, F. Maran. Metal Doping of $Au_{25}(SR)_{18}^{-}$ Clusters: Insights and Hindsights. *Journal of the American Chemical Society.* 2019, **141,** 16033-16045.
[32] C. García, S. Pollitt, M. van der Linden, V. Truttmann, C. Rameshan, R. Rameshan, E. Pittenauer, G. Allmaier, P. Kregsamer, M. Stöger-Pollach, N. Barrabés, G. Rupprechter. Support effect on the reactivity and stability of $Au_{25}(SR)_{18}$ and $Au_{144}(SR)_{60}$ nanoclusters in liquid phase cyclohexane oxidation. *Catalysis Today.* 2019, **336,** 174-185.
[33] K. Kwak, W. Choi, Q. Tang, M. Kim, Y. Lee, D.-e. Jiang, D. Lee. A molecule-like $PtAu_{24}(SC_6H_{13})_{18}$ nanocluster as an electrocatalyst for hydrogen production. *Nature Communications.* 2017, **8,** 14723.
[34] R. Jin, K. Nobusada. Doping and alloying in atomically precise gold nanoparticles. *Nano Research.* 2014, **7,** 285-300.
[35] S. Hossain, Y. Imai, D. Suzuki, W. Choi, Z. Chen, T. Suzuki, M. Yoshioka, T. Kawawaki, D. Lee, Y. Negishi. Elucidating ligand effects in thiolate-protected metal clusters using $Au_{24}Pt(TBBT)_{18}$ as a model cluster. *Nanoscale.* 2019, **11,** 22089-22098.
[36] H. Qian, D.-e. Jiang, G. Li, C. Gayathri, A. Das, R.R. Gil, R. Jin. Monoplatinum Doping of Gold Nanoclusters and Catalytic Application. *Journal of the American Chemical Society.* 2012, **134,** 16159-16162.
[37] S.L. Christensen, M.A. MacDonald, A. Chatt, P. Zhang, H. Qian, R. Jin. Dopant Location, Local Structure, and Electronic Properties of $Au_{24}Pt(SR)_{18}$ Nanoclusters. *The Journal of Physical Chemistry C.* 2012, **116,** 26932-26937.
[38] M.G. Taylor, G. Mpourmpakis. Rethinking Heterometal Doping in Ligand-Protected Metal Nanoclusters. *The Journal of Physical Chemistry Letters.* 2018, **9,** 6773-6778.
[39] Y. Negishi, T. Iwai, M. Ide. Continuous modulation of electronic structure of stable thiolate-protected Au_{25} cluster by Ag doping. *Chemical Communications.* 2010, **46,** 4713-4715.
[40] Y. Niihori, S. Hossain, B. Kumar, L.V. Nair, W. Kurashige, Y. Negishi. Perspective: Exchange reactions in thiolate-protected metal clusters. *APL Materials.* 2017, **5,** 053201.
[41] M. Walter, J. Akola, O. Lopez-Acevedo, D. Jadzinsky Pablo, G. Calero, J. Ackerson Christopher, L. Whetten Robert, H. Grönbeck, H. Häkkinen. A unified view of ligand-protected gold clusters as superatom complexes. *Proceedings of the National Academy of Sciences.* 2008, **105,** 9157-9162.
[42] M.A. Tofanelli, C.J. Ackerson. Superatom Electron Configuration Predicts Thermal Stability of $Au_{25}(SR)_{18}$ Nanoclusters. *Journal of the American Chemical Society.* 2012, **134,** 16937-16940.

[43] H. Häkkinen. Electronic shell structures in bare and protected metal nanoclusters. *Advances in Physics: X.* 2016, **1,** 467-491.
[44] M.A. Tofanelli. Applications of superatom theory in metal cluster chemistry. *Journal.* 2016.
[45] K.L.D.M. Weerawardene, P. Pandeya, M. Zhou, Y. Chen, R. Jin, C.M. Aikens. Luminescence and Electron Dynamics in Atomically Precise Nanoclusters with Eight Superatomic Electrons. *Journal of the American Chemical Society.* 2019, **141,** 18715-18726.
[46] I. Shun. Collision-Induced Reductive Elimination of 1,3-Diynes from $[MAu_{24}(C{\equiv}CR)_{18}]^{2-}$ (M = Pd, Pt) Yielding Clusters of Superatoms. *Journal of Physical Chemistry.* 2020, **124,** 19119-19125.
[47] M. Zhou, H. Qian, M.Y. Sfeir, K. Nobusada, R. Jin. Effects of single atom doping on the ultrafast electron dynamics of $M_1Au_{24}(SR)_{18}$ (M = Pd, Pt) nanoclusters. *Nanoscale.* 2016, **8,** 7163-7171.
[48] V.D. Thanthirige, M. Kim, W. Choi, K. Kwak, D. Lee, G. Ramakrishna. Temperature-Dependent Absorption and Ultrafast Exciton Relaxation Dynamics in $MAu_{24}(SR)_{18}$ Clusters (M = Pt, Hg): Role of the Central Metal Atom. *The Journal of Physical Chemistry C.* 2016, **120,** 23180-23188.
[49] M. Zhou, C. Yao, M.Y. Sfeir, T. Higaki, Z. Wu, R. Jin. Excited-State Behaviors of $M_1Au_{24}(SR)_{18}$ Nanoclusters: The Number of Valence Electrons Matters. *The Journal of Physical Chemistry C.* 2018, **122,** 13435-13442.
[50] F. Maran. Personal Communication. 2022.
[51] M. Ebina, T. Iwasa, Y. Harabuchi, T. Taketsugu. Time-Dependent Density Functional Theory Study on Higher Low-Lying Excited States of $Au_{25}(SR)_{18}^{-}$. *The Journal of Physical Chemistry C.* 2018, **122,** 4097-4104.
[52] G. te Velde, F.M. Bickelhaupt, E.J. Baerends, C. Fonseca Guerra, S.J.A. van Gisbergen, J.G. Snijders, T. Ziegler. Chemistry with ADF. *Journal of Computational Chemistry.* 2001, **22,** 931-967.
[53] M. Zhu, W.T. Eckenhoff, T. Pintauer, R. Jin. Conversion of Anionic $[Au_{25}(SCH_2CH_2Ph)_{18}]-$ Cluster to Charge Neutral Cluster via Air Oxidation. *The Journal of Physical Chemistry C.* 2008, **112,** 14221-14224.
[54] G.U. Kuda-Singappulige, P.S. Window, C.A. Hosier, I.D. Anderson, C.M. Aikens, C.J. Ackerson. Chiral and Achiral Crystal Structures of $Au_{25}(PET)_{18}^{0}$ Reveal Effects of Ligand Rotational Isomerization on Optoelectronic Properties. 2022, Submitted.
[55] E. van Lenthe, A. Ehlers, E.-J. Baerends. Geometry optimizations in the zero order regular approximation for relativistic effects. *The Journal of Chemical Physics.* 1999, **110,** 8943-8953.
[56] J.J. Goings, J.M. Kasper, F. Egidi, S. Sun, X. Li. Real time propagation of the exact two component time-dependent density functional theory. *The Journal of Chemical Physics.* 2016, **145,** 104107.
[57] J.P. Perdew. Density-functional approximation for the correlation energy of the inhomogeneous electron gas. *Physical Review B.* 1986, **33,** 8822-8824.
[58] A.D. Becke. Density-functional exchange-energy approximation with correct asymptotic behavior. *Physical Review A.* 1988, **38,** 3098-3100.
[59] S.J.A. van Gisbergen, J.G. Snijders, E.J. Baerends. Implementation of time-dependent density functional response equations. *Computer Physics Communications.* 1999, **118,** 119-138.

[60] M. Seth, G. Mazur, T. Ziegler. Time-dependent density functional theory gradients in the Amsterdam density functional package: geometry optimizations of spin-flip excitations. *Theoretical Chemistry Accounts.* 2011, **129,** 331-342.
[61] K. Kwak, Q. Tang, M. Kim, D.-e. Jiang, D. Lee. Interconversion between Superatomic 6-Electron and 8-Electron Configurations of $M@Au_{24}(SR)_{18}$ Clusters (M = Pd, Pt). *Journal of the American Chemical Society.* 2015, **137,** 10833-10840.
[62] M.A. Tofanelli, K. Salorinne, T.W. Ni, S. Malola, B. Newell, B. Phillips, H. Häkkinen, C.J. Ackerson. Jahn–Teller effects in $Au_{25}(SR)_{18}$. *Chem Sci.* 2016, **7,** 1882-1890.
[63] K.L.D.M. Weerawardene, C.M. Aikens. Theoretical Insights into the Origin of Photoluminescence of $Au_{25}(SR)_{18}^{-}$ Nanoparticles. *Journal of the American Chemical Society.* 2016, **138,** 11202-11210.
[64] X. Lin, X. Fu, Y. Yang, X. Ren, J. Tang, C. Liu, J. Huang. Synthesis and Optical Properties of Unique Pt_1Ag_{24} Nanoclusters with Mixed Exterior Motif Structures. *Inorganic Chemistry.* 2021, **60,** 10167-10172.